PROCEEDINGS OF SPIE

SPIEDigitalLibrary.org/conference-proceedings-of-spie

Sensitivity analysis of a multibranched light guide for real time hyperspectral imaging systems

Craig M. Browning, Samuel Mayes, Joshua Deal, Arslan Arshad, Samantha Gunn Mayes, et al.

Craig M. Browning, Samuel Mayes, Joshua Deal, Arslan Arshad, Samantha Gunn Mayes, Marina Parker, Thomas C. Rich, Silas J. Leavesley, "Sensitivity analysis of a multibranched light guide for real time hyperspectral imaging systems," Proc. SPIE 10871, Multimodal Biomedical Imaging XIV, 1087107 (27 February 2019); doi: 10.1117/12.2510506



Event: SPIE BiOS, 2019, San Francisco, California, United States

Sensitivity analysis of a multibranched light guide for real time hyperspectral imaging systems

Craig M. Browning^{1,2}, Samuel Mayes^{1,2}, Joshua Deal^{3,4}, Arslan Arshad¹, Samantha Gunn Mayes¹,
Marina Parker^{1,2}, Thomas C. Rich^{3,4}, Silas J. Leavesley^{1,3,4}

¹Chemical and Biomolecular Engineering, University of South Alabama, AL 36688

²Systems Engineering, University of South Alabama, AL 36688

³Pharmacology, University of South Alabama, AL 36688

⁴Center for Lung Biology, University of South Alabama, AL 36688

ABSTRACT

Hyperspectral imaging (HSI) is a spectroscopic technique which captures images at a high contrast over a wide range of wavelengths to show pixel specific composition. Traditional uses of HSI include: satellite imagery, food distribution quality control and digital archaeological reconstruction. Our lab has focused on developing applications of HSI fluorescence imaging systems to study molecule-specific detection for rapid cell signaling events or real-time endoscopic screening.

Previously, we have developed a prototype spectral light source, using our modified imaging technique, excitation-scanning hyperspectral imaging (HIFEX), coupled to a commercial colonoscope for feasibility testing. The 16 wavelength LED array was combined, using a multi-branched solid light guide, to couple to the scope's optical input. The prototype acquired a spectral scan at near video-rate speeds (~8 fps). The prototype could operate at very rapid wavelength switch speeds, limited to the on/off rates of the LEDs (~10 µs), but imaging speed was limited due to optical transmission losses (~98%) through the solid light guide. Here we present a continuation of our previous work in performing an in-depth analysis of the solid light guide to optimize the optical intensity throughput. The parameters evaluated include: LED intensity input, geometry (branch curvature and combination) and light propagation using outer claddings. Simulations were conducted using a Monte Carlo ray tracing software (TracePro). Results show that transmission within the branched light guide may be optimized through LED focusing lenses, bend radii and smooth tangential branch merges. Future work will test a new fabricated light guide from the optimized model framework.

Keywords: Endoscopy, Colonoscopy, Colorectal Cancer, Light Emitting Diode, Spectroscopy

1. INTRODUCTION

Colorectal cancer is the 3rd highest ranked cancer in mortality and incidence rates in the United States. ^{1–3} The gold standard for screening colorectal cancer is white light endoscopy using a colonoscope. A possible correlation to high ranking colorectal cancer is the reduced accuracy of detecting small and/or flat lesions in the colorectum.^{4,5} The major limitation of detecting these small/flat lesions is the low contrast to the surrounding mucosa.^{6–8} Detection then depends on the experience of the endoscopist for noticing subtle visual differences between a suspected lesion and surrounding mucosa. Additionally, current techniques provide little to no capabilities to determine the risk of the detected lesion (invasive potential or sessile, serrated markers linked to metastasis) or to render a diagnosis such as hyperplastic. precancerous or carcinoma. Alternative imaging techniques have been tested to increase detection accuracy within endoscopy including: narrow-band imaging and autofluorescence imaging. Narrow-band imaging (NBI) illuminates the mucosa with blue and green light to enhance the vasculature. Vasculature density differences can represent lesion or normal tissue (higher density correlates to adenomas). Studies show a 10-20% increase in detection sensitivity but decreased specificity of 5-10% providing only marginal, if any, improvement over standard white light endoscopy. 6,7 Autofluorescence imaging (AFI) excites the tissue with short wavelengths of light and the emission spectra (normally a longer wavelength) is collected to determine the differences in tissue. However, the studies using AFI result in little to no improvements for detection accuracy. ⁶ The techniques represented here use either broad spectrum light (white light endoscopy) or single channel illumination (narrow-band or autofluorescence) attempting to generate enhanced contrast

Multimodal Biomedical Imaging XIV, edited by Fred S. Azar, Xavier Intes, Qianqian Fang, Proc. of SPIE Vol. 10871, 1087107 ⋅ © 2019 SPIE ⋅ CCC code: 1605-7422/19/\$18 ⋅ doi: 10.1117/12.2510506

between lesions and the surrounding mucosa. In light of the limited or negligible improvements offered by alternative imaging modalities, new imaging approaches need to be developed to discriminate abnormal growths from the mucosa in a high-contrast manner and to provide feedback in order to diagnose a lesion or other region of interest (i.e. inflammation, ulcerative colitis or Crohn's disease). 9,10

Here we present a technique which harnesses spectroscopic data during a screening process to visually enhance and contrast the image feed and provide quantitative results through spectroscopic differences acquired with the images. This technique is hyperspectral imaging (HSI); which images a two-dimensional area over a spectral range collecting a threedimensional spectral image cube with component specific spectra per pixel. Hyperspectral imaging is historically significant in remote sensing of satellite or drone imagery showing agricultural differences in terrain and crops (i.e. nutrients monitoring and pest control). Other applications include food processing, 13 historical art and documentation restoration 14,15 and archaeology. 16 While there are many alternative approaches for analyzing HSI data, the ability to determine relative abundances of either individual molecules or cancer-correlated signatures would provide enhanced contrast for optical diagnosis within endoscopy. We have previously reported on the ability to perform HSI on a microscope platform using a novel HSI technique, excitation-scanning hyperspectral imaging. 17-20 This technique acquires the full emission spectra at every excitation wavelength (vs. acquiring key emission peaks by filtering the reflected or fluorescence emission spectra). We have also recently reported a prototype device implementing this technique in a light source which couples to a commercially accepted endoscope. ^{21,22} This spectral light source used light emitting diodes (LED) of specific wavelengths for excitation instead of a broad spectrum source and tunable filter array. 17 This allowed us to further increase acquisition speeds through electronic triggering of LEDs instead of mechanical switching of filters. Preliminary bench testing of the hyperspectral endoscopic system provided moderate resolution reflectance images at sub-video rates (~8 fps). This was due to the transmission losses (~98%) through our multi-furcated solid light guide design. The solid light guide was designed to collimate and combine multiple individual LEDs to a common output which couples to the illumination optics of the endoscope. The preliminary design was implemented for the proof-of-concept work mentioned above. The results showed the theoretical capability of this technique using a LED source, however, in order to achieve the desired image quality at video rates (20-30 fps) the optical throughput needed to increase. Here we present a theoretical optimization and design to improve the efficiency of the branched solid light guide. This in turn should allow acquisition of hyperspectral images in real time video format for optical discrimination of lesions and the mucosa as well as provide quantitative data to determine the predicted risk (normal, precancerous or cancerous) through the spectral signatures collected in the images of the lesion, with the end goal of increasing the detection accuracy of early stage colorectal cancer using a real-time HSI endoscopy system.

2. METHODS

2.1 Solid Light Guide Component Modeling

An alpha prototype system was developed for proof-of-concept in using the excitation-scanning HSI technique within the field of endoscopy. The alpha version contained a 16-channel branched solid light guide of optical grade acrylic to combine the respective LEDs (Figure 1). The resulting device was capable of microsecond interval wavelength cycling allowing for millisecond spectral image cube scans. However, the optical efficiency of the alpha prototype was limited and there was a trade-off between acquisition time and the intensity of light collected per scan. The low transmission required longer acquisition times to capture the majority of the light per wavelength. A compromise was to operate at the fastest acquisition speeds to visualize distinguishable vascular patterns. The acquisition speeds resulted in 100-200 ms allowing for 8 fps video speeds. It should be noted that the framerate represents the speed to acquire the spectral image cube not individual wavelength frames. This initial work demonstrates the need for an optimized beta prototype to acquire real time hyperspectral image data on endoscopic samples (i.e. swine colon or cadavers). The transition to robust bench testing and future clinical trials mandates consideration of the beta prototype on a larger scale and how it will fit into the screening process through the entire product lifecycle. The hyperspectral endoscopic system needs to be considered holistically including the needs and the desires of physicians and patients. This led us to the design a multifurcated solid light guide to not only increase optical intensity throughput but consider the maintainability, usability and safety of the component. Design aspects we determined to consider throughout the modeling and manufacturing of this light guide include: the number of wavelengths needed in an array, the minimum area needed for each LEDs circuit and heat dissipation, the ability to maintain a planar design (to not combine branches from another plane) to reduce complexity for cost and replacement (maintainability) and additional modifications to increasing internal reflectance or cladding for increased transmission as well as safety for the user. Other components and aspects are under consideration simultaneously with the optimization of the solid light guide, however, that discussion is beyond the scope of this paper.

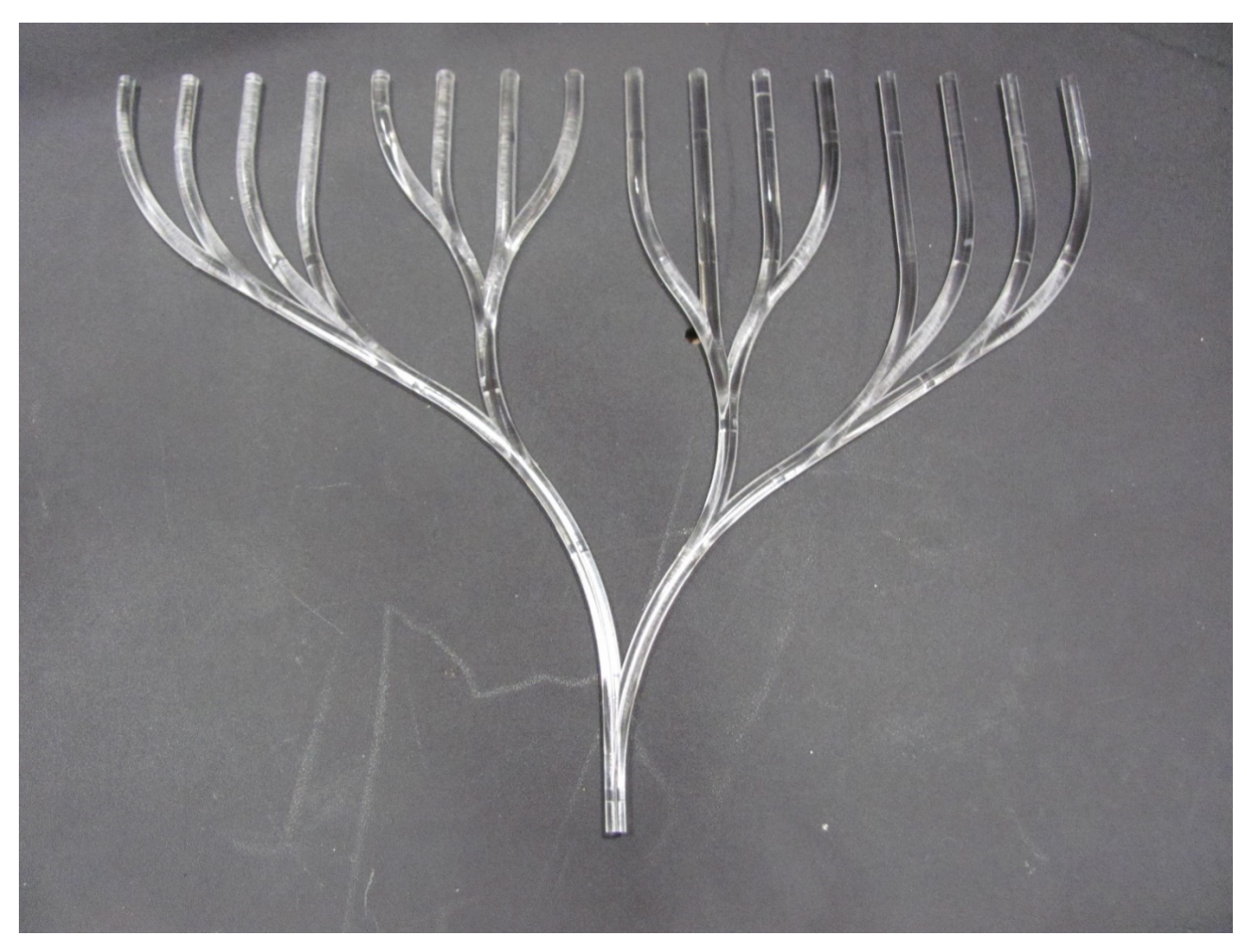


Figure 1: The alpha prototype multi-furcated optical grade acrylic solid light guide

The optimization of the solid light guide began with modeling various designs in a raytracing software (TracePro, Lambda Research) for optical intensity simulation measurements. TracePro software uses a Monte Carlo analysis by projecting a ray of light from the emitter (LED) in a randomized vector and reports the probability (of all the rays traced) of the amount of light collected (on the detection surface called an Exit Surface) as a function of the amount of light emitted by the illumination source (e.g., fractional or percent transmission). Current models consist of an emitter, the solid light guide design in the form of a pipe and a detection surface. The emitting surface has input parameters that match the intensity, shape, angle and wavelength of commercial LEDs used in the alpha prototype (SMB1N-525V-02, Roithner LaserTechnik). The size of the emitter matches the dimensions of the physical LED. The light pipe is 5 mm in diameter (the same as the LED and the previous light guide iteration) with input properties of acrylic plastic. The detector is the same 5 mm in diameter to match the light pipe and resemble the input of the endoscope. The detection surface is marked as an Exit Surface (to measure % transmission) and a perfect absorber at this time to reduce the possibility of back reflection and creating a false transmission measurement. The distances between LED and pipe and pipe and detector are 1 mm and 2 mm respectively to simulate the physical distance between these entities. These parameters and positions are all to simulate the physical version, both the alpha and beta prototype.

The simulation modeling process was designed to begin with simple geometries and build complexity as the modeling advances and more channels are added. Testing by simulation was used: to reduce costs associated with multiple redesigns, to improve speed of the overall system design process, and to verify results from the initial alpha prototype to validate the model accuracy. The simulation process varies one or more independent variables (i.e. pipe diameter or pipe length) through a parametric sensitivity study. 100,000 rays were traced for all simulations except as noted. For each value of the independent variable, an irradiance map was produced of the detection surface showing the surface

distribution of incident rays as an intensity plot and calculating the % transmission. Concurrently, polar, iso-polar and rectangular distribution plots were produced at the exit surface of the light pipe to show the shape, distribution and angular distribution of the light exiting the pipe. The distribution plots were compiled to compare the distribution differences between the entrance and exit surface of the light pipe and the mirrored distribution of the irradiance map. The irradiance maps were normalized to the emitted flux of the LED and the distributions were normalized to the maximum intensity produced during the entire set of parameter values. This process was repeated for every value of the independent variable for the entire cycle. These simulations and simulation data collection were conducted through the use of individual macro loops. The following independent variables have been evaluated thus far: pipe diameter, pipe length, pipe curvature (angle and radius of the curve) and pipe bend (angle to compare to pipe curve). Here, we describe the simulation results from comparison of the pipe curve and bend. Additionally, some simulation verification results are included to show the efficacy of the simulations and models.

3. RESULTS AND DISCUSSION

3.1 Ray Tracing Simulations

The alpha prototype (Figure 1) provided a basis for the modeling and design of an optimized solid light guide. Combining LED channels to a single output requires evaluation of the optical effects of light pipe curvature and junction points. Here we focused on a single channel curve or bend to determine the optimal geometric parameter values for combining light from multiple LEDs (Figure 2 and Figure 3). The simulation loop for a single pipe curve varied the angle of the revolving curve and the radius of the revolving circle (increasing radius of revolution increased the arc length of the curved pipe). The range of angle iterations comprised of 15-90° every 15° with a maximum of 90° to avoid counteracting the overall linear path from LED to endoscope. Revolution radii spanned 10-100 mm every 10 mm and 100-1000 mm every 100 mm to determine optimal size and monitor if there was a plateau in optical throughput.

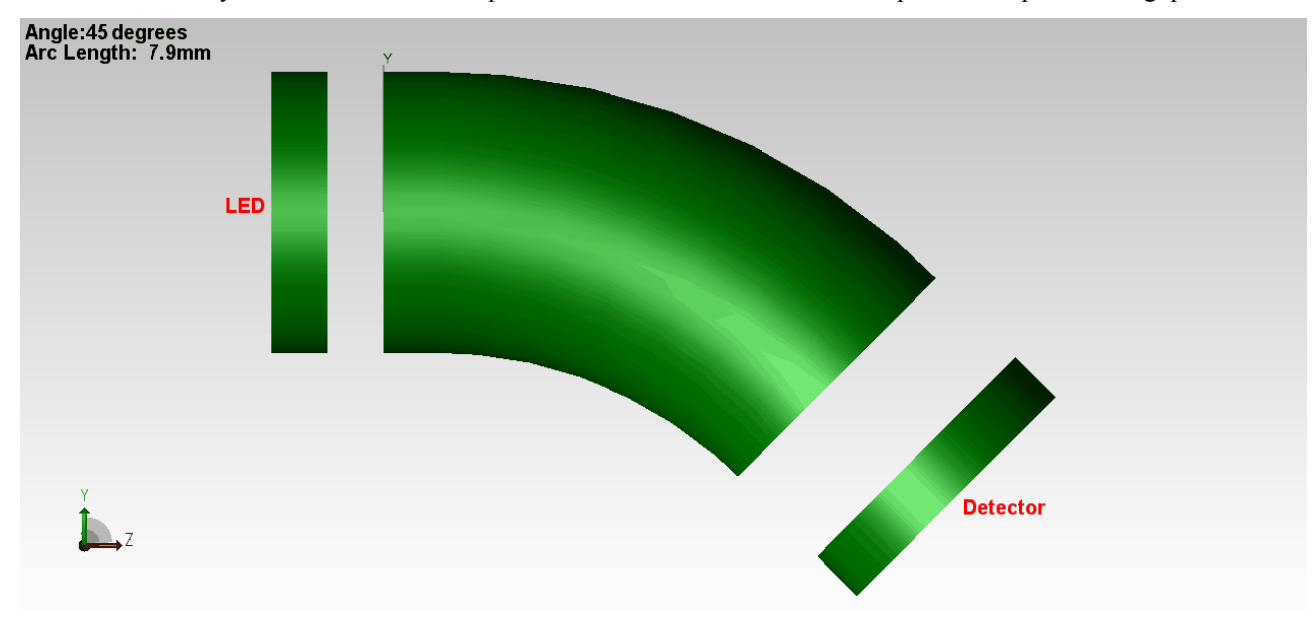


Figure 2: "Pipe Curve Angle_45" Pipe curve model of 45° over the radius of revolution range. The arc length is used in the figures for comparison. The radius of the pipe remains 5 mm for all iterations the size changes due to the relative size of the frame to fit a longer arc length pipe. http://dx.doi.org/10.1117/12.2510506

The simulations for the light pipe bend followed a similar scenario. The angle range remained the same for comparison to the light pipe curve. For the light pipe bend, however, the arc length (using the revolution radius) was calculated for each iteration of the curve loop and that arc length was equally divided on either side of the bend to equate the arc length to that of the pipe curve (accounting for the length of the bend) for comparison. Figure 3 is an example of a pipe bend iteratation that is comparable to curved geometry shown in Figure 2.

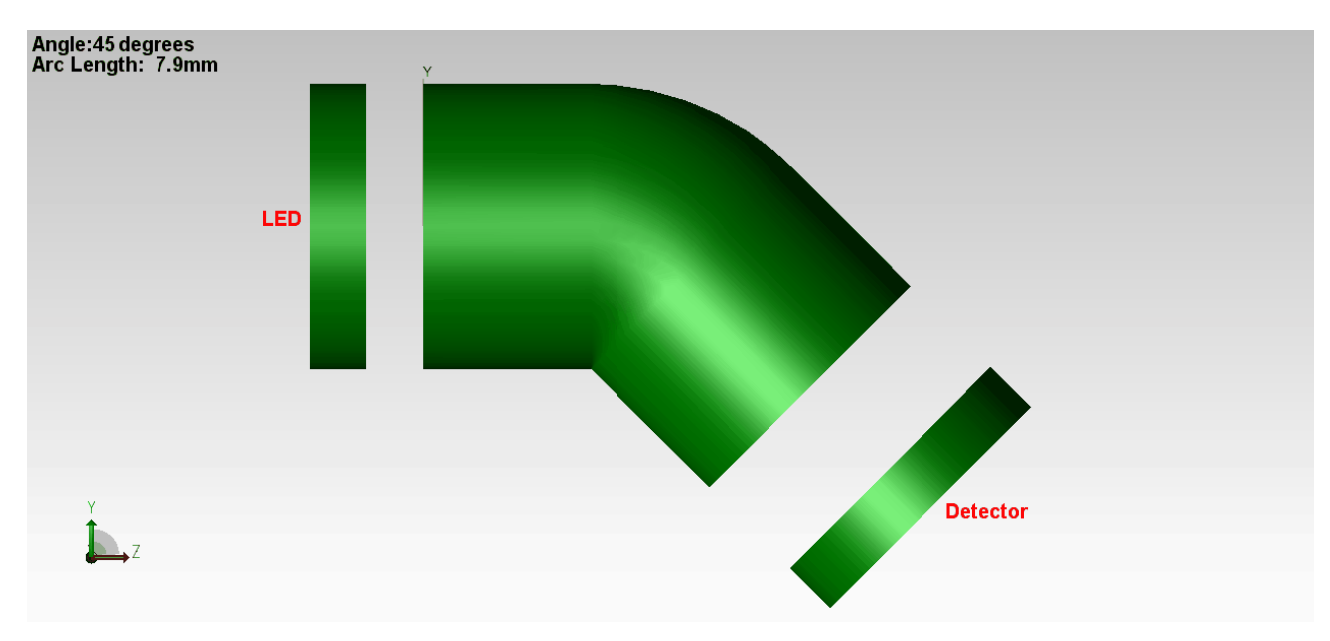


Figure 3: "Pipe Bend Angle_45" Pipe bend model of 45° over the range of lengths which associate to the radii of the pipe curve for equivalent arc lengths. The radius of the pipe remains 5 mm for all iterations the size changes due to the relative size of the frame to fit a longer arc length pipe. http://dx.doi.org/10.1117/12.2510506

The irradiance map intensity data was compiled for each value of the independent variable (Figure 4). The % transmission was categorized by angle and displayed over the range of revolution radii for the curve and similar distances for the bend).

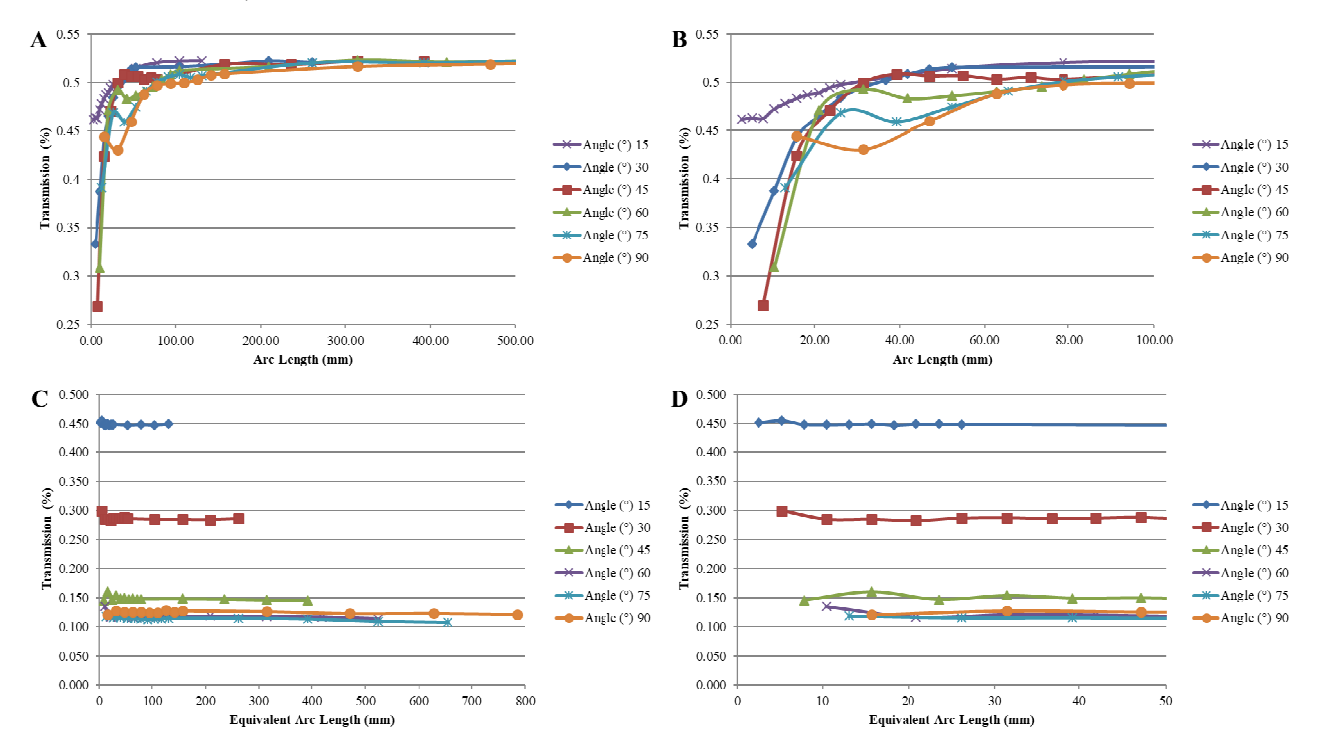


Figure 4: Comparison of the optical lightpipe curve and bend models showing optical transmission as a function of % transmission vs. total pipe length. (A) Results from the light pipe curve model over the entire range of arc radii, (B) an expanded view of the first ten iterations of panel A to visualize the overlapping data, (C) results from the light pipe bend model over the entire range of equivalent arc radii and (D) an expanded view of the first ten iterations to visualize the overlapping data.

Intensity data, as measured at the interrogation plane, shows that a curved light pipe geometry is provides higher optical transmission than a bent pipe. The optimal bend in a pipe was 15° regardless of the arc radius of the pipe. Every other angle produced a reduced optical transmission not suitable for consideration this early in the modeling process. The curved light pipe geometry maintained ~50% transmission at any angle as long as the arc length was approximately 100 mm. For the 60° , 75° and 90° arc angles, the calculated optical transmission displayed an unusual decrease in optical transmission as the arc radius increased, which occurred at a radius value of between 20-40 mm. At this point, any angle of sufficient arc radius would be of utility in the design of the beta light pipe. Further testing of a double curve, where the pipe curves back to the original direction, will aid in determining the optimal angle and arc length for the beta design.

Throughout the simulation coding and modeling process, some verification measures were included to ensure that the software model accurately predicted the physical reality. Model validation included comparing the input parameters of the model LED to the physical measurements and determining if the number of rays traced in the simulation provided an accurate representation of the data (transmission or distribution). The experimentally-measured irradiance properties of the 525 nm LED and the model results for intensity and distribution were in strong agreement of 97% using the full width half maximum (FWHM) for measurement comparison (Figure 5)

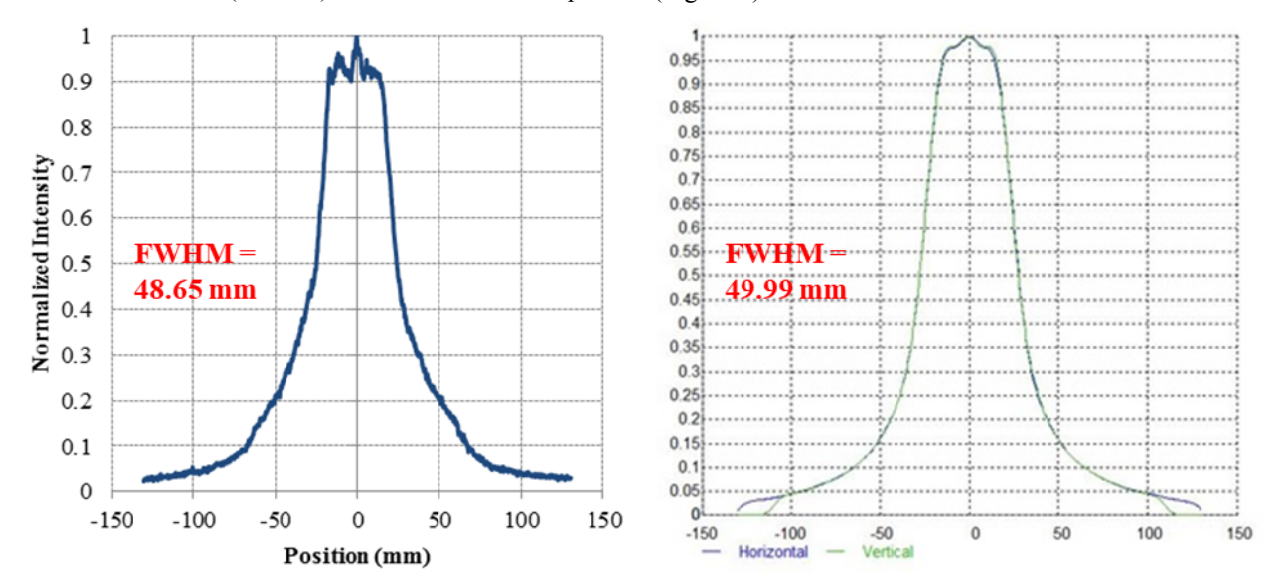


Figure 5: A comparison of the 525 nm LED (left) physical irradiance characteristics measured with a spectrometer and (right) TracePro simulation of the LED model. Experimental data were acquired by projecting the LED beam profile onto grid paper a fixed distance from the LED. Theoretical data were generated by projecting the simulated LED source onto a flat interrogation plane at the same fixed distance from the LED.

Verifying the number of rays needed to produce an accurate measurement consisted of using a single model (a single set of independent parameter values) and increasing the number of rays traced from 100,000 rays to 1,000,000 rays and 5,000,000 rays. Results indicate that 100,000 rays is sufficient to estimate the % transmission at the interrogation plane with similar values as produced by the greatly increased ray counts. However, the advantage to increased rays is the increased accuracy of the irradiance and candela maps (Figure 6), which require a sufficient number of rays to be traced to accurately sample the irradiance at each position and angle of the interrogation plane.

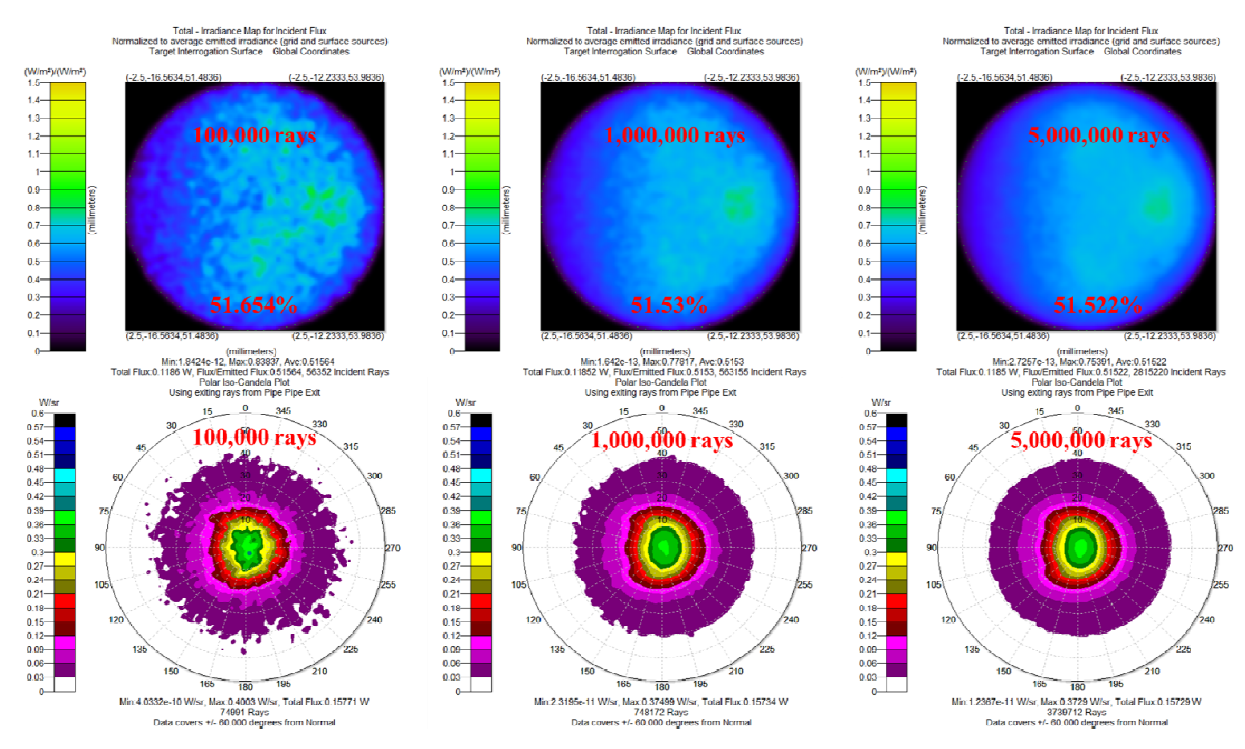


Figure 6: Verification of the number of rays to determine the accuracy of the measurements for (top) the irradiance map of the curved light pipe model – angle of revolution 30°, radius of revolution 100 mm and (bottom) polar iso candela plot of the curved light pipe model – angle of revolution 30°, radius of revolution 100 mm

4. FUTURE WORK

The work presented here illustrates the compromises that must be made during the first phase of the optical system design process. Phase I focused on single channel variations to determine the optimal size and shape of channels for the solid light pipe. Phase II will consist of combining channels to measure the optical intensity as transmitted through a junction point. This appears to be one of the major sources of light loss in the alpha prototype. Models will include: a straight pipe with a curved second pipe junction, two curved pipes in junction and the various angles and positions needed to determine an optimal configuration. Phase III will focus on designing a final version of the multifurcated solid light guide with a minimum of 16 channels. In addition to light guide simulation, we are evaluating the design of the entire HSI system to accommodate the future light guide while increasing maintainability and usability for clinical testing. Fluorescent biomarkers and interactions are also planned to better define the potential contrast generated by the HSI endoscopy system.^{23,24} This work supports the overall goal to achieve improved detection accuracy for colorectal cancer, especially early stage small and/or flat lesions.

5. ACKNOWLEDGEMENTS

The authors would like to acknowledge support from NIH grant numbers UL1 TR001417, P01 HL066299, NSF grant number 1725937, the Abraham Mitchell Cancer Research Fund, the University of Alabama at Birmingham Center for Clinical and Translational Science (CCTS), and the Economic Development Partnership of Alabama. Drs. Leavesley and Rich disclose financial interest in a start-up company, SpectraCyte LLC, founded to commercialize spectral imaging technologies.

REFERENCES

- [1] Siegel, R., Desantis, C., and Jemal, A., "Colorectal cancer statistics, 2014.," CA: a cancer journal for clinicians 64(2), 104–117 (2014).
- [2] Siegel, R.L., Miller, K.D., and Jemal, A., "Cancer statistics, 2016," CA: a cancer journal for clinicians 66(1), 7–30 (2016).
- [3] Siegel, R.L., Miller, K.D., and Jemal, A., "Cancer statistics, 2017," CA: A Cancer Journal for Clinicians 67(1), 7–30 (2017).
- [4] Rex, D.K., Cutler, C.S., Lemmel, G.T., Rahmani, E.Y., Clark, D.W., Helper, D.J., Lehman, G.A., and Mark, D.G., "Colonoscopic miss rates of adenomas determined by back-to-back colonoscopies," Gastroenterology 112(1), 24–28 (1997).
- [5] van Rijn, J., Reitsma, J., Stoker, J., Bossuyt, P., van Deventer, S., and Dekker, E., "Polyp miss rate determined by tandem colonoscopy: a systematic review.," The American journal of gastroenterology 101(2), 343 (2006).
- [6] Ignjatovic, A., East, J., Guenther, T., Hoare, J., Morris, J., Ragunath, K., Shonde, A., Simmons, J., Suzuki, N., et al., "What is the most reliable imaging modality for small colonic polyp characterization? Study of white-light, autofluorescence, and narrow-band imaging.," Endoscopy 43(2), 94–99 (2011).
- [7] Chiu, H.-M., Chang, C.-Y., Chen, C.-C., Lee, Y.-C., Wu, M.-S., Lin, J.-T., Shun, C.-T., and Wang, H.-P., "A prospective comparative study of narrow-band imaging, chromoendoscopy, and conventional colonoscopy in the diagnosis of colorectal neoplasia," Gut 56(3), 373–379 (2007).
- [8] Togashi, K., Osawa, H., Koinuma, K., Hayashi, Y., Miyata, T., Sunada, K., Nokubi, M., Horie, H., and Yamamoto, H., "A comparison of conventional endoscopy, chromoendoscopy, and the optimal-band imaging system for the differentiation of neoplastic and non-neoplastic colonic polyps.," Gastrointestinal endoscopy 69(3 Pt 2), 734 (2009).
- [9] Bousvaros, A., Antonioli, D., Colletti, R., Dubinsky, M., Glickman, J., Gold, B., Griffiths, A., Jevon, G., Higuchi, L., et al., "Differentiating ulcerative colitis from Crohn disease in children and young adults: report of a working group of the North American Society for Pediatric Gastroenterology, Hepatology, and Nutrition and the Crohn's and Colitis Foundation of America.," Journal of pediatric gastroenterology and nutrition 44(5), 653–674 (2007).
- [10] Zappa, M., Stefanescu, C., Cazals-Hatem, D., Bretagnol, F., Deschamps, L., Attar, A., Larroque, B., Tréton, X., Panis, Y., et al., "Which magnetic resonance imaging findings accurately evaluate inflammation in small bowel Crohn's disease? A retrospective comparison with surgical pathologic analysis:," Inflammatory Bowel Diseases 17(4), 984–993 (2011).
- [11] Mulla, D.J., "Twenty five years of remote sensing in precision agriculture: Key advances and remaining knowledge gaps," Biosystems Engineering 114(4), 358–371 (2013).
- [12] Lee, W.S., Alchanatis, V., Yang, C., Hirafuji, M., Moshou, D., and Li, C., "Sensing technologies for precision specialty crop production," Computers and Electronics in Agriculture 74(1), 2–33 (2010).
- [13] Sun, D.-W., [Hyperspectral imaging for food quality analysis and control], Elsevier (2010).
- [14] Goltz, D., Attas, M., Young, G., Cloutis, E., and Bedynski, M., "Assessing stains on historical documents using hyperspectral imaging," Journal of cultural heritage 11(1), 19–26 (2010).
- [15] Kim, S.J., Zhuo, S., Deng, F., Fu, C.-W., and Brown, M., "Interactive visualization of hyperspectral images of historical documents," IEEE transactions on visualization and computer graphics 16(6), 1441–1448 (2010).
- [16] Cavalli, R.M., Licciardi, G.A., and Chanussot, J., "Detection of anomalies produced by buried archaeological structures using nonlinear principal component analysis applied to airborne hyperspectral image," IEEE Journal of Selected Topics in Applied Earth Observations and Remote Sensing 6(2), 659–669 (2013).

- [17] Favreau, P., Hernandez, C., Lindsey, A.S., Alvarez, D.F., Rich, T., Prabhat, P., and Leavesley, S.J., "Thin-film tunable filters for hyperspectral fluorescence microscopy," Journal of biomedical optics 19(1), 011017–011017 (2014).
- [18] Favreau, P.F., Hernandez, C., Heaster, T., Alvarez, D.F., Rich, T.C., Prabhat, P., and Leavesley, S.J., "Excitation-scanning hyperspectral imaging microscope," Journal of biomedical optics 19(4), 046010–046010 (2014).
- [19] Leavesley, S.J., Walters, M., Lopez, C., Baker, T., Favreau, P.F., Rich, T.C., Rider, P.F., and Boudreaux, C.W., "Hyperspectral imaging fluorescence excitation scanning for colon cancer detection," Journal of Biomedical Optics 21(10), 104003–104003 (2016).
- [20] Deal, J., Mayes, S., Browning, C., Hill, S., Rider, P., Boudreaux, C., Rich, T.C., and Leavesley, S.J., "Identifying molecular contributors to autofluorescence of neoplastic and normal colon sections using excitation-scanning hyperspectral imaging," Journal of Biomedical Optics 24(2), 021207 (2018).
- [21] Browning, C.M., Mayes, S., Favreau, P., Rich, T.C., and Leavesley, S.J., "LED-based endoscopic light source for spectral imaging," presented at SPIE BiOS, 2016, 97031I-97031I.
- [22] Browning, C.M., Mayes, S., Rich, T.C., and Leavesley, S.J., "Design of a modified endoscope illuminator for spectral imaging of colorectal tissues," presented at Proc. of SPIE Vol, 2017, 1006015–1.
- [23] Favreau, P.F., Deal, J.A., Weber, D.A., Rich, T.C., and Leavesley, S.J., "Assessment of autofluorescent signatures in multiple tissue types with novel excitationscanning hyperspectral imaging," The FASEB Journal 30(1 Supplement), 51–1 (2016).
- [24] Deal, J.A., Favreau, P., Weber, D., Rich, T., and Leavesley, S., "Potential of Hyperspectral Imaging for Label-free Tissue and Pathology Classification," The FASEB Journal 30(1 Supplement), 51–2 (2016).